https://doi.org/10.5194/esurf-2021-92
Preprint. Discussion started: 2 December 2021

Earth Surface Dynamics Discussions
Open Access
EGU

Linking levee-building processes with channel avulsion: Geomorphic analysis for assessing avulsion frequency and style

Jeongyeon Han[1] and Wonsuck Kim[1]

[1]Department of Earth System Sciences, Yonsei University, Seoul, 03722, Republic of Korea

Correspondence to: Wonsuck Kim (delta@yonsei.ac.kr)

Abstract. A natural levee is a typical wedge-shaped deposit adjacent to a river channel. Given its location and distinctive features, the levee can serve as a key to revealing depositional processes of the coupled channel to floodplain system preserved in the rock record. Levee-floodplain topographic evolution is also closely linked to river avulsion processes which can spell a catastrophic flood. Nonetheless, the levee geometry and its aggradation pattern on the floodplain have not been fully incorporated in the study of avulsion. Here, we present a levee-building model using an advection settling of suspended sediment to reproduce the evolution of a fluvial levee over floods and to examine the effects of boundary conditions on levee geometry and grain-size trend. We further investigate river avulsion frequencies and styles (i.e., local vs. regional avulsion) associated with the grain-size distribution of supplied sediment and the overflow velocity into the floodplain, which control the levee geometry and especially the aggradation rate at the levee crest. In the modelling results, the levee develops 1) a concave-up profile, 2) exponentially decreasing grain size in the deposit, and 3) a relatively steeper shape for coarser sediment supply. The subsequent scaling analysis supports that the input grain size and levee profile slope are positively correlated with the avulsion frequency, whereas the overflow velocity is inversely proportional to the avulsion frequency. In connection with the avulsion styles and levee geometry, we suggest that steeper levee slopes tend to promote more local avulsions protecting abandoned channels from topographic healing, but gentler slopes of the levee are likely to lead to regional avulsions as abandoned channels with gentler levees are more vulnerable to the removal of topographic memory. The insights drawn from the current modelling work may thus have potential implications for reconstructing paleoenvironments in regard to river sediment transport and flood processes via levee deposits. Based on the roles of a levee on the avulsion frequency and style, the flood hazards triggered by river avulsions as well as the alluvial architecture in sedimentary records can be better assessed.

1 Introduction

During floods, rivers overflow into floodplains, facilitating the deposition of suspended sediment on account of the loss of flow competence and transport capacity. The reduction in competence and capacity are responsible for the decreases in depositional rate and grain size away from the rivers and form distinctive wedge-shaped natural levees along the channel margins. Because of their unique location at the boundary, levees may represent an important linkage between the mainstream

https://doi.org/10.5194/esurf-2021-92
Preprint. Discussion started: 2 December 2021

and overbank processes (Allen, 1965; Brierley et al., 1997; Wolman and Leopold, 1957). According to Brierley et al. (1997), this linkage between the channel and floodplain facies could further play a critical role in assessing river types that cover geometry, size, and distribution of the channel deposits in stratigraphic records.

Despite the geomorphologic and stratigraphic importance of levee deposits, there have been only a limited number of publications to address the fluvial levee deposition process. Indeed a few early numerical models of suspended sediment transport and depositional processes in floodplains have been carried out. These models include James (1985) and Pizzuto (1987), which quantify the suspended sediment deposition and grain-size distribution across the channel margin to the floodplain and have been a great aid in comprehending the mechanisms of overbank configuration. Similarly, some studies have probed detailed evolution of levee geometry based on the field investigations of natural levees (Adams et al., 2004; Cazanacli and Smith, 1998; Ferguson and Brierley, 1999; Filgueira-Rivera et al., 2007; Gugliotta et al., 2018; Johnston et al., 2019; Pierik et al., 2017; Skolasińska, 2014; Smith and Pérez-Arlucea, 2008). Cazanacli and Smith (1998) described geometry and lateral grain-size distributions of fluvial levees, where the differences in levee shape and slope are attributed to non-uniform deposition of coarse overbank sediment. Ferguson and Brierley (1999) stated that the stream power decided by valley width is essential for levee accretion and floodplain stripping, and thus the preservation potential of levee deposits. Recent work by Pierik et al. (2017) underlined that dimensions of levees and their changes in time are associated with both environmental forcing (e.g., suspended sediment influx and flood intensity) and initial geomorphic conditions (e.g., flood basin configurations). Even with the earlier achievements, there is still a need to ascertain the primary driver of levee geomorphology in order to accurately delineate and interpret field data of modern river systems and ancient fluvial records. In particular, it is necessary to analyse the effects of geometry and depositional rate of fluvial levees on the stratal association of channel-floodplain complexes.

Moreover, there have been no attempts to establish a fluvial levee-building model accounting for the river avulsion process, which would be also an important step forward to understand the influence of natural levees in connecting in-channel and floodplain evolution. River avulsion, an abrupt relocation of a river from an established channel to a fresh or formerly abandoned channel, is one of the important processes for river dynamics and fluvial stratigraphy. It has long been known that the channel perching with an increment in potential energy leads to lateral instability, which subsequently increases the likelihood of channel avulsion (Bryant et al., 1995; Imran et al., 1998; Mohrig et al., 2000). After multiple floods, alluvial ridges can simultaneously be accumulated as much as the in-channel deposits and serve as local superelevation, the relief between levee crest and minimum low point of the nearby floodplain (Bryant et al., 1995; Heller and Paola, 1996; Mohrig et al., 2000). The study by Mohrig et al. (2000) suggested that comparing channel depth with levee crest height (i.e., normalized superelevation) can be regarded as an avulsion criterion. According to those authors, the river would be avulsed when the levee crest height exceeds approximately one channel depth. Some researchers have recently proved that even climate change and anthropogenic effects such as land use and deforestation, can enforce dramatic changes in channel avulsion behaviours and increase the possibilities of catastrophic flooding disasters in densely populated communities near river systems (Chadwick et al., 2020; Mishra and Sinha, 2020; Pearce, 2021; Slingerland and Smith, 2004). Yet, the comprehension of river avulsion

https://doi.org/10.5194/esurf-2021-92
Preprint. Discussion started: 2 December 2021

Earth Surface Dynamics Discussions
Open Access
EGU

associated with floodplain architecture, especially with levee morphology is still insufficient. With these concerns in mind, it would be a great task to unravel the relationship between river switching and levee-building processes linked to the flood conditions for predicting modern avulsion processes and diminishing the threats posed by avulsion flooding events (Valenza et al., 2020).

In this study, we develop an advection-settling, suspended sediment transport model to quantitatively determine what are the main controls on geometry, depositional rate, and grain-size sorting in fluvial levee evolution during flooding. A total of five tests are conducted, in which the overflow velocity, grain size, entrainment, and the condition of water level are varied. We then explore river avulsion frequencies and styles associated with the levees constructed differently under the various input sediment grain sizes and flood-flow discharges and demonstrate the contributions of levee deposits to the mechanisms governing the river avulsion behaviours with respect to their geomorphic and sedimentary processes.

2 Mathematical model

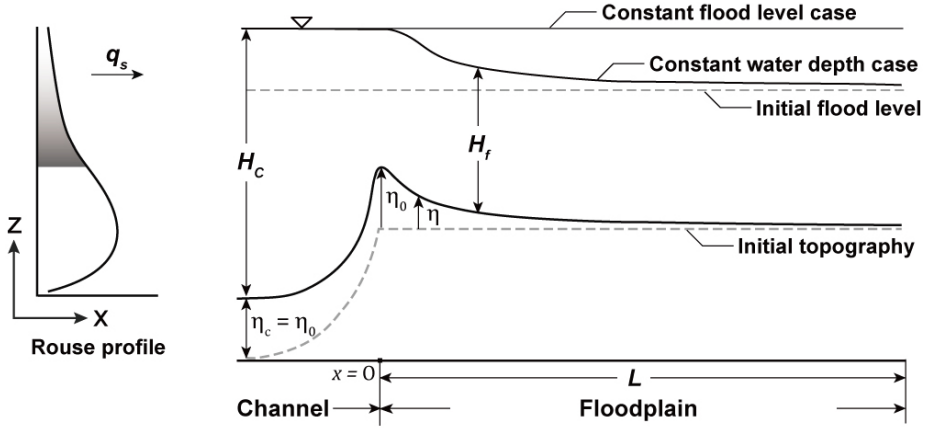

Figure 1. Schematic of a levee with the Rouse profile used in the model. The extent of suspended sediment supplied to the floodplain (q_s) is grey coloured on the Rouse profile. Note that the upstream end of the model is assigned at the channel-floodplain boundary as the origin (x = 0) where the levee crest develop and the downstream direction of the model is towards the distal floodplain, to which x increases.

2.1 1D levee building model

Consider an initially flat floodplain adjacent to a flooded channel, the overflow carries suspended sediment from the channel to the floodplain, and the suspended sediment is settled down to build a levee (Fig. 1). The mass conservation of suspended sediment takes the following form as:

$$H\frac{\partial \bar{C}_{fi}}{\partial t} = -\frac{\partial q_{si}}{\partial x} + (E_{si} - D_{si}) - \bar{C}_{fi}\frac{\partial H}{\partial t}, \quad (1)$$

https://doi.org/10.5194/esurf-2021-92
Preprint. Discussion started: 2 December 2021

where H is the depth of overflow in the floodplain, the subscript i represents the ith grain size range, $\bar{C}_f$ denotes the average suspended sediment concentration (SSC) in the flood flow, q_s denotes the volume transport of suspended sediment per unit width, E_s and D_s are the entrainment and deposition rates per unit width, respectively. This governing equation calculates the change in SSC for each grain-size range with time.

The total sediment flux at the channel-floodplain boundary (at the boundary between the channel margin and the floodplain), q_{so} depends on the distribution of SSC in the channel. We use the Rouse equation (Rouse, 1937) to illustrate the vertical sediment concentration profile in the channel and integrate the concentration profile to produce q_{so} only over the depth between the levee crest and water surface. The Rouse equation is written as:

$$\frac{\bar{C}_{ci}}{\bar{C}_{ai}} = \left(\frac{\frac{H_c - z}{z}}{\frac{H_c - a}{a}}\right)^{P_i}, \tag{2}$$

$$P_i = \frac{w_{si}}{\kappa u_*}, \tag{3}$$

where $\bar{C}_{ci}$ is the sediment concentration for the ith grain size range at elevation z, $\bar{C}_{ai}$ denotes the near bed concentration at $z = a$, and H_c is the channel depth. In this model, we adopt a reference near bed height as $a = 0.05H_c$, proposed in Garcia and Parker (1991) and assume the grain-size distribution of suspended sediment to be normally distributed with a standard deviation of $\sigma = 0.8$. The Rouse profile in the channel depends on the total sediment flux of the channel (q_{ts}) and the near bed concentration ($\bar{C}_{ai}$), and both are kept constant with time. P_i denotes the dimensionless Rouse number for the ith grain-size range in which w_{si} denotes the settling velocity, κ is the von Karman constant of 0.41, and u_* is the shear velocity. We apply the settling velocity (w_{si}) equation as $w_{si} = Rgd_i^{\,2}/[C_1\nu + (0.75C_2Rgd_i^{\,3})^2]$ in Ferguson and Church (2004) where the grain-shape constants are $C_1 = 18$ and $C_2 = 1$ for natural grains; R is submerged specific gravity; g is gravitational acceleration; d_i is the ith grain size range; and ν is the kinematic viscosity of fluid.

We make an erodible substrate at the beginning, supposing suspended sediment in the initial flood flow to be uniformly mixed and settled over the entire floodplain instantaneously (i.e., the time for levee deposition is much longer than that for flood inundation over the floodplain.). The initial concentration of suspended sediment in the floodplain can be defined as:

$$\bar{C}_{fi}[t = 0] = \alpha \frac{q_{soi}}{U_f \cdot H_f}, \tag{4}$$

where α denotes a constant ($\alpha = 0$ for fresh flood water and $\alpha > 0$ for an initial sediment concentration) which we set at $\alpha = 1$ for simplicity. U_f and H_f denote the initial flow velocity and depth in the floodplain, respectively.

The depositional rate for the ith grain-size range D_{si} is described as a function of settling velocity and the concentration of suspended sediment:

$$D_{si} = w_{si}\bar{C}_{bi}, \tag{5}$$

https://doi.org/10.5194/esurf-2021-92
Preprint. Discussion started: 2 December 2021

in which $\bar{C}_{bi}$ is the near bed concentration in the floodplain. The near bed concentration of floodplain is defined as $\bar{C}_{bi} = \beta \bar{C}_{fi}$,
115 where β is a dimensionless factor and assumed unity for simplicity.

For the entrainment rate of the ith grain-size range E_{si}, the relations of Garcia and Parker (1991) for non-uniform sediment are employed. The relations can be expressed as:

$$E_{si} = w_{si} E_i, \tag{6}$$

$$E_{ui} = \frac{E_i}{F_i} = \frac{A {Z_{ui}}^5}{1 + \frac{A}{0.3} {Z_{ui}}^5}, \tag{7}$$

120 where E_{ui} is the dimensionless entrainment rate of the ith grain-size range per unit area, F_i denotes the ith grain-size fraction entrained from the bed, and A is a constant set at $A = 1.3 \times 10^{-7}$. According to Garcia and Parker (1991), the similarity variable for the ith grain-size range, Z_{ui} can be written as:

$$Z_{ui} = \lambda_m \frac{u_{*s}}{w_{si}} {Re_{pi}}^{0.6} \left(\frac{d_i}{d_{50}}\right)^{0.2}, \tag{8}$$

where $Re_{pi} = \sqrt{Rgd_i} d_i / w_{si}$ is Reynold's particle number for the ith grain-size range; $\lambda_m = 1 - 0.298\sigma$, where σ denotes
125 the arithmetic standard deviation of the surface sediment in the grain size scale ψ; u_{*s} is the shear velocity associated with skin friction; and d_{50} is the median grain size on the sediment surface.

Combining the governing equation, Eq. (1) with the Exner equation of conservation of bed sediment yields the following form for the time evolution of the bed elevation $\eta[x, t]$ as:

$$\left(1 - \lambda_p\right) \frac{\partial \eta}{\partial t} = D_s - E_s. \tag{9}$$

130 This indicates that the topographic elevation is a product of a balance between the entrainment and settling of suspended sediment. The study assumes that all suspended sediment in the floodplain is deposited without any porosity ($\lambda_p = 0$) to be more straightforward. We note that these assumptions and simplifications can be relaxed in the future, more elaborate model.

2.2 Test parameters

In order to test our numerical model, we apply field-scale parameters obtained from previous studies in the Vistula
135 River at the Smolice station, southern Poland (Pruszak et al., 2005; Wyżga, 1999). The dimensions of the channel and floodplain have been chosen based on the field observations of natural levee deposits in the Vistula River (Wyżga, 1999). The slopes of the channel and floodplain in the model were assigned the same as $S_c = S_f = 10^{-4}$. A constant overflow depth in the floodplain (H_f) of 4 m was employed, with a channel depth (H_c) of 8 m. The flow velocity (U_c) in the channel and overflow velocity in the floodplain (U_f) were kept at constant values of 1.5 m/s and 0.1 m/s, respectively.

140 Equation (3) is used for defining an overbank sediment flux at the channel-floodplain boundary, q_{so}. It is assumed that the elevations of the main channel bed and levee crest increase simultaneously at the same aggradation rate so that input

https://doi.org/10.5194/esurf-2021-92
Preprint. Discussion started: 2 December 2021

Earth Surface Dynamics Discussions
Open Access
EGU

SSC entering the floodplain remains constant in the model (Fig. 1). We approximate the total suspended sediment flux in the channel (q_{ts}) of 0.001 m^2/s and allocate it to SSCs for seven different grain sizes at the channel near bed with the median grain size (d_{50}) of 0.125 mm. Fig. 2 shows the grain-size distribution of suspended sediment both for the near-bed channel and for the floodplain supplied at the channel-floodplain boundary. The fractions of each grain size and the cumulative distributions are represented in Fig. 2a and 2b, respectively. We observe in both figures, that the incoming sediments to the floodplain are finer than SSC in the channel because only the suspended sediments above the levee crest elevation are taken to transport to the floodplain. We also assign the extent of inundation as a floodplain width (L) of 200 m. The width is divided into 20 grid nodes (N) in the model and each node stores modelling results of topographic elevation, grain size, and SSC to analyze their spatial and temporal trends from the proximal to distal locations.

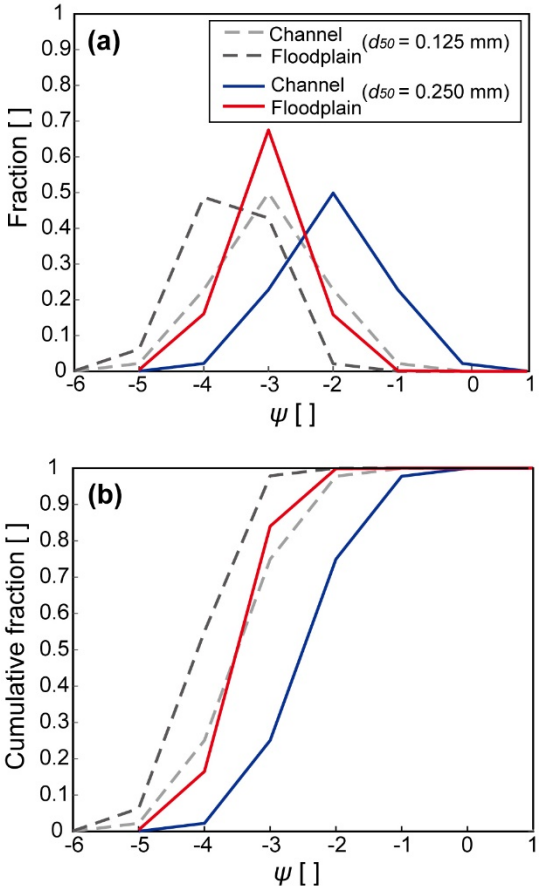

Figure 2. (a) Grain-size distribution curves and (b) cumulative grain-size distributions of suspended sediments at near bed and at channel-floodplain boundary. Dotted lines are for channel (grey) and floodplain (black) when d_{50} = 0.125 mm and solid lines are for channel (blue) and floodplain (red) when d_{50} = 0.250 mm, respectively.

https://doi.org/10.5194/esurf-2021-92
Preprint. Discussion started: 2 December 2021

Earth Surface Dynamics Discussions
Open Access
EGU

2.3 Test setup

The main purpose of our test model is to gain the first-order understanding of the fluvial levee evolution under various but simple boundary conditions. We focused on changes in the levee profile associated with the overbank flow velocity and the median grain size of suspended sediments. We also dealt with the effects of entrainment and flood water level on the levee evolution and stratigraphic development in our model. All these parameters are summarized in Table 1. A total of 5 tests were performed until the levee crest in each run (at the upstream end of the floodplain) reaches 2 m. The total simulation times (T) were different in the runs in response to various depositional rates at the levee crest calculated with the varied boundary conditions. Based on the adapted parameters from a field example, we set a prototype model as Test 1. To estimate the entrainment effect, Test 2 contained the entrainment relations of Garcia and Parker (1991) in Eq. (7) and (8). The case of constant water depth in the prototype model was compared to the constant flood level case in Test 3 (Fig. 1). Test 4 was simulated with 1.5 times higher flood flow velocity than that in Test 1. We doubled the median grain size (d_{50}) of SSC at the channel near bed from 0.125 mm in Test 1 to 0.25 mm in Test 5. Fig. 2 depicts the grain-size distributions of Tests 1 and 5 at the channel and the floodplain. The model produced the formation of a levee in the cross-sectional view and could predict the proximal to distal grain-size distribution in the levee deposits. The final surface profiles and the time series of surface elevation changes at the proximal (grid node $N = 3$) and distal (grid node $N = 15$) locations were captured. We then plotted the grain-size fining trends in the distal direction and the grain-size changes over time at the proximal and distal locations. All modelling results are shown against the results from the prototype model (Test 1) to identify the differences.

Table 1. **Initial boundary conditions for the 5 Test runs.**

Test	U_f	d_{50}	E	T
1	0.1	0.125	-	7,733
2	0.1	0.125	Relations of Garcia and Parker (1991)	8,575
3	$U(x, t)$	0.125	-	7,733
4	0.15	0.125	-	10,942
5	0.1	0.250	-	9,341

U_f = Average flow velocity on floodplain [m s^{-1}].

d_{50} = Median grain size of suspended sediment in channel [mm].

T = Simulation time [minute].

E = Entrainment [ ].

https://doi.org/10.5194/esurf-2021-92
Preprint. Discussion started: 2 December 2021

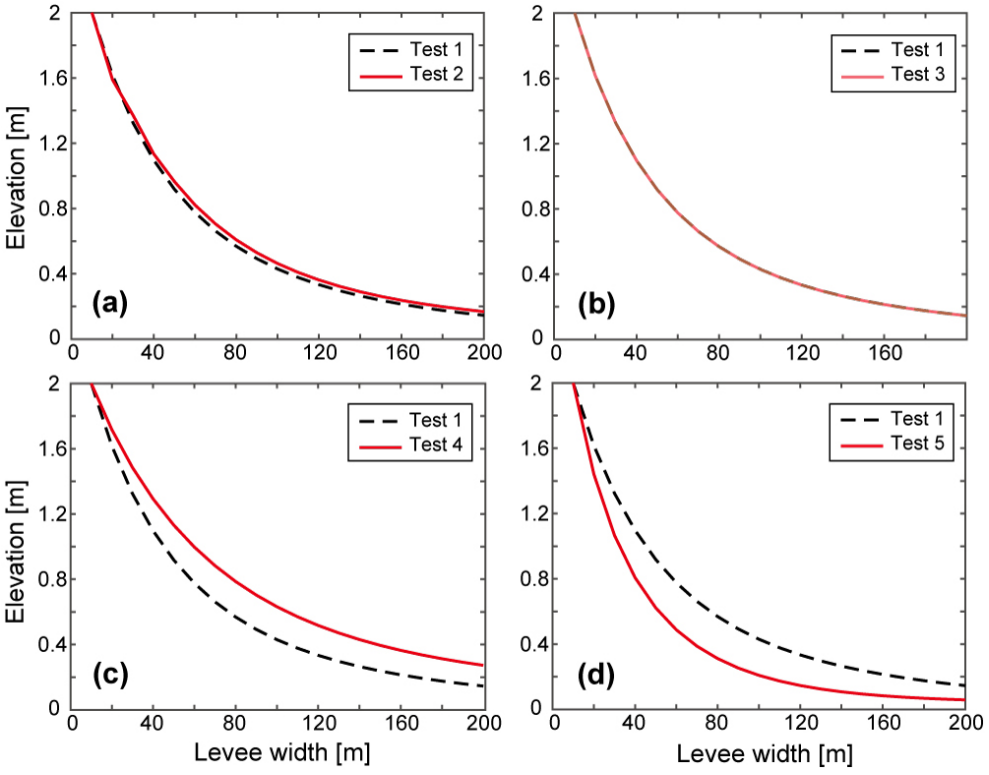

Figure 3. Levee surface profiles taken at the end of each model. The black dotted line represents the results of Test 1 and the red lines are other test results.

3 Modelling results

3.1 Levee profile

The cross-sectional views of predicted levee topography are presented in Fig. 3. The black dotted and red lines are the results of the prototype model (Test 1) and other test runs, respectively. The elevation of Test 2 at the proximal distance near the levee crest was slightly lower than Test 1, whereas, at the distal locations, Test 2 has slightly higher elevations (Fig. 3a). However, the differences (caused by the entrainment) are not significant. In Fig. 3b, the results do not indicate any noticeable differences between Tests 1 and 3 with the difference flood level conditions. The total simulation times for both two models are also the same (Table 1). The levee profile of Test 4 using a higher flood velocity, shown in Fig. 3c, is gentler in slope and takes a longer time to build up the levee crest of 2 m. Test 5 with an increase in grain size produces a steeper slope of levee despite the longer total run time compared with Test 1 (Fig. 3d).

https://doi.org/10.5194/esurf-2021-92
Preprint. Discussion started: 2 December 2021

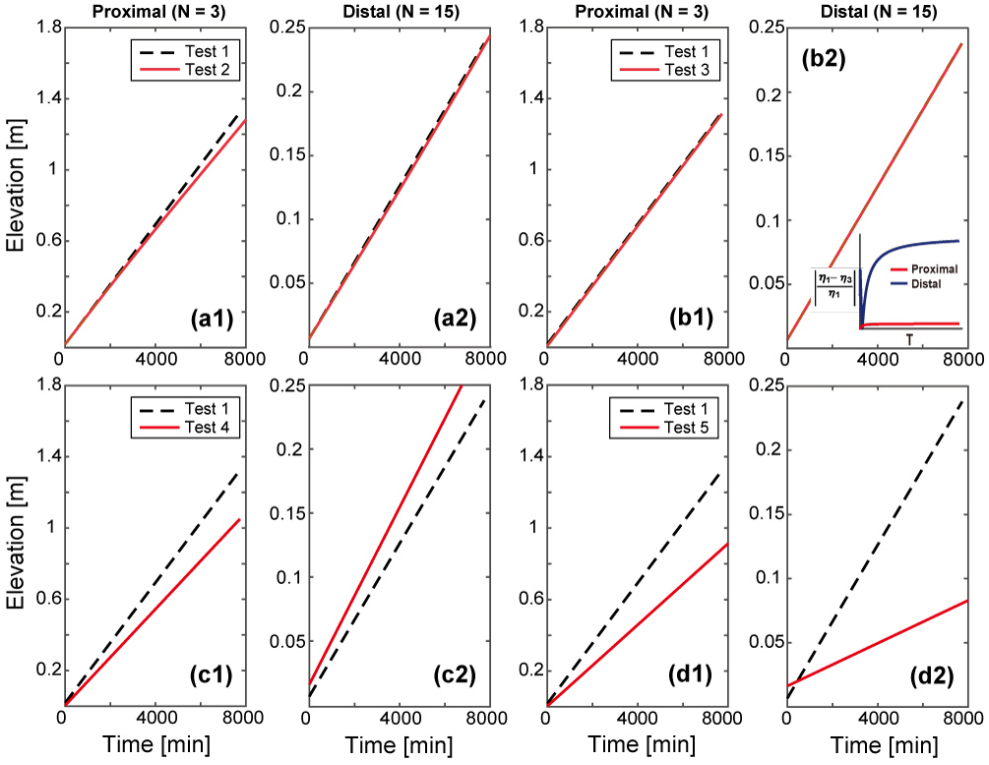

Figure 4. Time series of levee elevations at the proximal (N = 3, x = 30 m) and distal (N = 15, x = 150 m) locations (red solid lines) against the results of Test 1 (black dotted lines). At each location, the scales of the two y-axes differ by (a) up to 1.8 m for the proximal and (b) 0.25 m for the distal location. In (b), we additionally plot the normalized ratio of elevation differences between Tests 1 and 3 ($\left|\frac{\eta_1-\eta_3}{\eta_1}\right|$) over time both at the proximal and distal locations.

3.2 Temporal variations of levee elevation

Figure 4 indicates changes in the levee surface elevation over time at the proximal location (grid node N = 3) and the distal location (N = 15) and suggests that the local surface elevations increase linearly. In terms of the aggradation rate, the gradients of the prototype model are 0.1689 × 10^{-3} m/min and 0.0299 × 10^{-3} m/min at the proximal and distal positions, respectively. Each test result presents deviations from the results of the prototype although the slopes (aggradation rates) for Tests 2 and 3 are not significantly deviating from Test 1 (Figs. 4a and 4b). The depositional rates for Test 3 at both locations are lower than Test 1, and the normalized differences between Tests 1 and 3 are higher at the distal location than that of the proximal location (Fig. 4b). In Fig. 4c, the slope of the plot for the proximal location in Test 4 is lower than that of the prototype model, while the slope at the distal location is steeper than prototype one, which represents that the increase in the flood-flow velocity enhances deposition in the distal locations. Meanwhile, the depositional rates of Test 5 with coarser sediment inputs both at the proximal and distal locations become lower than those of the Test 1 model (Fig. 4d).

https://doi.org/10.5194/esurf-2021-92
Preprint. Discussion started: 2 December 2021

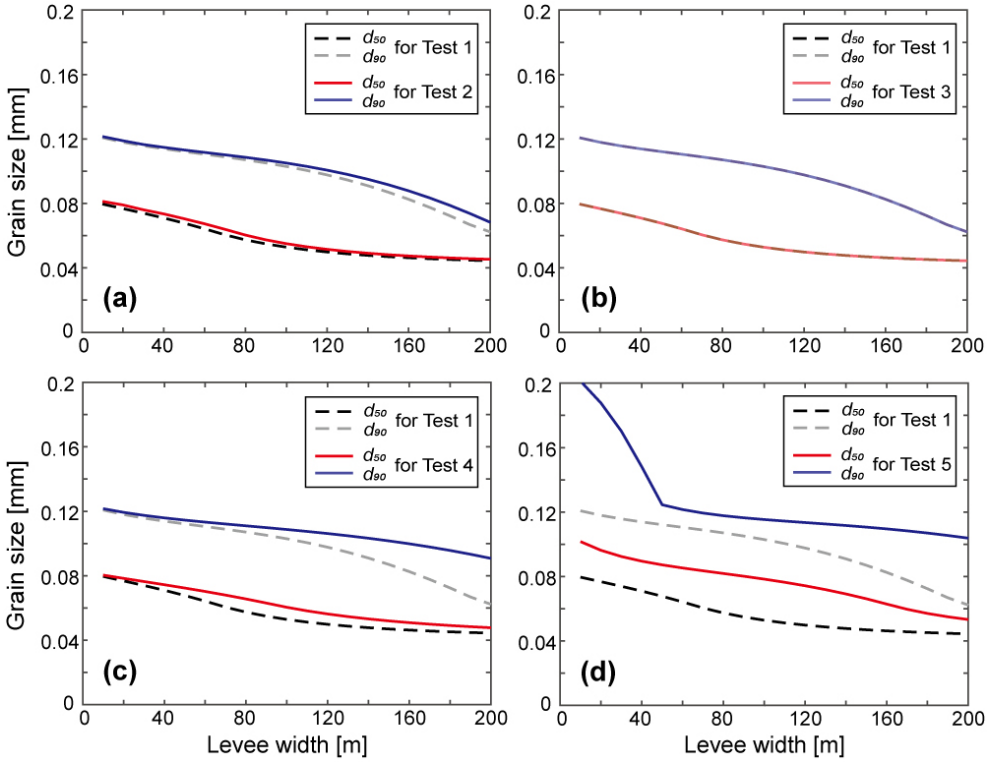

Figure 5. The grain-size (d_{50} and d_{90}) curves for the predicted levee deposits as a function of the distance from the channel-floodplain boundary. The two solid lines (red and blue) represent d_{50} and d_{90} for each tests and the dotted lines (black and grey) are for Test 1, respectively.

3.3 Spatial trends in grain size of levee deposit

The plots of variations in grain sizes d_{50} (median grain size) and d_{90} (90 % finer grain size) versus distance from the channel-floodplain boundary show that the grain sizes decrease from the proximal to distal locations in general, which allow us to identify various downstream fining trends (Fig. 5). Except for Tests 4 and 5, d_{50} decreases from 0.08 to 0.04 mm and d_{90} changes from 0.12 to 0.06 mm over the 200-m width. Also, the reduction of d_{50} is relatively smooth as it approaches a specific value (0.04 mm) from the middle of the levee, whereas d_{90} keeps decreasing in the distal positions. In Fig. 5c, compared to Test 1, the d_{50} and d_{90} values in Test 4 are generally coarser, especially at the distal locations. In Fig. 5c, d_{90} decreases only by 0.03 mm across the levee. For Test 5 that has a coarser grain-size distribution, both d_{50} and d_{90} drop further than any other runs with rollover points in d_{90} on the more proximal position than in d_{50} (Fig. 5d).

https://doi.org/10.5194/esurf-2021-92
Preprint. Discussion started: 2 December 2021

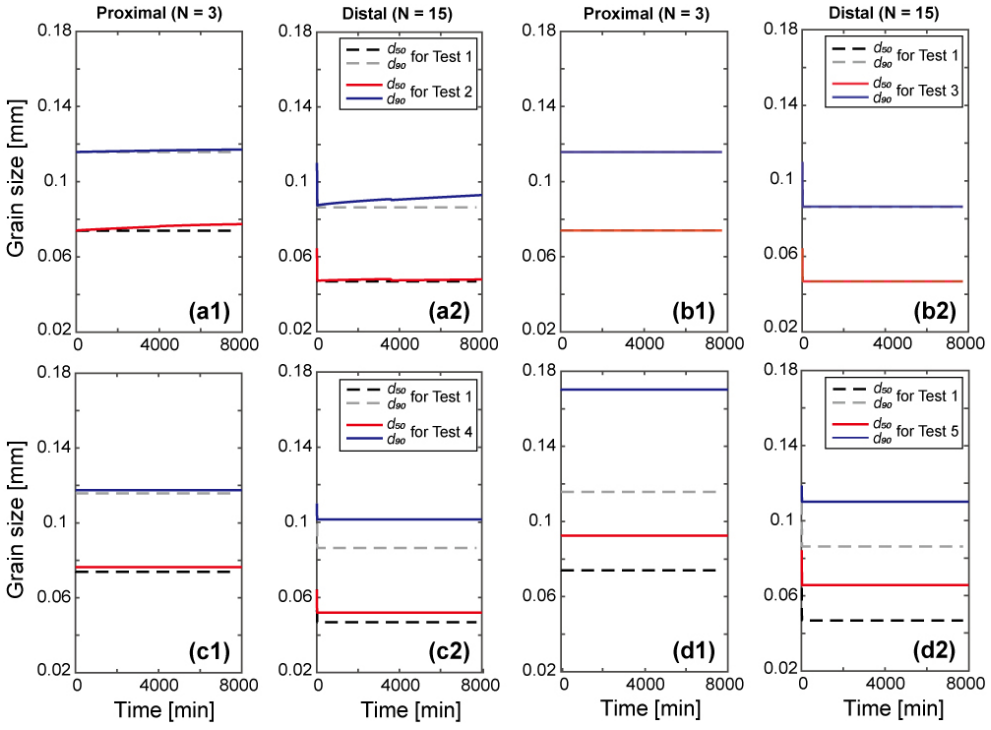

Figure 6. Time series of grain sizes d_{50} and d_{90} at the top levee surface at the proximal ($N = 3$, $x = 30$ m) and distal ($N = 15$, $x = 150$ m) locations. The red and blue solid lines indicate the grain sizes d_{50} and d_{90} for each test, and the black and grey dotted lines are for Test 1, respectively.

3.4 Temporal variations of grain size of levee deposit

The model calculates d_{50} and d_{90} at the top deposit layer and records them every timestep at the assigned proximal and distal locations of levees (Fig. 6). At both positions, the grain sizes d_{50} and d_{90} for most tests become finer quickly over the initial short run time and reach the equilibrium sizes except Test 2. The grain sizes in Test 2 rather increase over time, which can develop upward coarsening sequences (Fig. 6a). Test 3 has an overall similar fining pattern compared to the prototype result shown in Fig. 6b, but the grain-size values for all other tests are greater than Test 1. Both the prototype model and Test 3, the grain sizes d_{50} and d_{90} approach steady values of 0.0740 mm and 0.1158 mm at the proximal, 0.0469 mm and 0.0863 mm at the distal location, respectively. Fig. 6c represents the results of Test 4 and shows different increasing patterns of d_{50} and d_{90} between the proximal and distal locations. At the proximal position, the grain sizes of Test 4 progressively merges to coarser values than Test 1, and display that the difference in d_{50} from the prototype model of 0.0024 mm is greater than that in d_{90} of 0.0017 mm. On the other hand, at the distal location, the difference of d_{90} between the prototype and Test 4 (0.0153 mm) is nearly three times as high as that of d_{50} (0.0050 mm). Test 5 also shows generally coarser grain sizes than the prototype model (Fig. 6d). We can notice that the difference of d_{90} between Tests 1 and 5 at the proximal location (0.0544 mm) is greater than that of d_{50} (0.0185 mm), while the differences of d_{50} and d_{90} at the distal location are 0.0189 mm and

https://doi.org/10.5194/esurf-2021-92
Preprint. Discussion started: 2 December 2021

0.0239 mm, respectively, which are relatively smaller. In addition, at the distal locations for all the tests, there are sharp drops in the grain size at the beginning of the runs due to the substantial grain size decreasing associated with the time that takes until the supplied suspended sediment transports to the distal location.

4 Discussion

The model produces concave-up surface profiles and shows proximal to distal fining trends, both of which are the typical features of natural levees. Throughout the test runs, we found that the levee evolution is not very different from the prototype when the model used the entrainment or the flood level condition (Test 3). However, when the overflow velocity or the grain size of incoming suspended sediment to the floodplain increases, the levee shape significantly becomes gentler or steeper than the prototype model, respectively. Herein, we attribute the levee geometry and its grain-size trend to the variable external forcing, such as flood hydraulics and suspended sediment supply.

4.1 Entrainment

Test 2 using the entrainment of sediment from the bed is shown in (a)s from Fig. 3a to Fig. 6a. The aggradation rates for Test 2 are much lower at the proximal location but only slightly lower at the distal location compared to Test 1 and thus the final levee profile is slightly lower at the proximal part but higher at the distal part for the final elevations (Figs. 3a and 4a). The overall grain sizes, d_{50} and d_{90} also become coarser than Test 1 and increase with time at each location (Figs. 5a and 6a). These suggest that the deposits near the levee crest were reworked and resuspended due to the entrainment and then transported further to the distal location. In particular, resuspension of the sediment on the surface by entrainment is more preferential for finer grain sizes with smaller settling velocities as expressed in Eq. (7) and (8). The resuspended finer grains hence act more on d_{50} than d_{90} at the proximal location over time, which causes much clear upward coarsening sequences of d_{50} in Fig. 6a. On the contrary, at the distal location, d_{50} has relatively low rates of increase over time compared to the d_{90} as resuspended fines reaching the distal locations are more prone to bypass the levee width without settling.

4.2 Water level condition

The prototype model has a constant water depth across the evolving levee on the floodplain, thereby the water surface is in phase with the sediment-surface topography. In contrast, Test 3 is a case of the constant flood level which means the water elevation in the channel always defines the flood level across the floodplain (Fig. 1). Both test models use the advection settling of suspended sediment, but the setups in terms of the lateral water-surface slopes are similar to the “wide and dry” floodplain versus “narrow and wet” floodplains, two flooding styles reported in Adams et al. (2004), respectively. As the levee gradually grows in Test 3, the overflow depth at the levee crest is constant because the in-channel deposition is assumed to be equal to the levee crest aggradation. In this case, the flood depth increases further away from the levee crest and the flood

https://doi.org/10.5194/esurf-2021-92
Preprint. Discussion started: 2 December 2021

velocity decreases over time causing decreases in aggradation rates at the distal locations compared to Test 1 (Fig. 4b). However, in general, there are no meaningful changes between prototype and Test 3 in terms of the profile shape, aggradation rate, and grain-size distribution during the total run time until the levee crest reaches 2-m high (Fig. 3b through Fig. 6b). We inferred that in our model water level does not affect the topographic and grain-size characteristics of levee significantly in a way that increases in the water depth to the distal direction are compensated by decreases in the suspended concentration. Furthermore, if the flood level is equal everywhere in the floodplain, i.e., the hydraulic gradient is minimal so the flood flow should not be significant, and thus diffusion would be possibly dominant (Adams et al., 2004).

4.3 Overflow discharge

To evaluate the effect of hydraulic characteristics of flood in overbank deposits, we set that Test 4 has 1.5 times higher flood discharge which brings 1.5 times higher flow velocity at the channel-floodplain boundary since the water depth is kept constant (James, 1985; Pierik et al., 2017; Wyżga, 1999). The faster flow is more efficient to transport coarser sediment further into the floodplain on account of an increase its competence. It also results in higher aggradation rates at the distal part than that at the proximal part in comparison with those of the prototype model, which is reflected in the gentler levee-profile slope (Figs. 3c and 4c). The gentler slope in Test 4 produces a larger volume under the profile compared to that in Test 1, which implies it needs more time to be filled until the levee crest height reaches 2 m. In the same context, the faster flow with regard to the grain-size distribution over the levee has more influence on the coarser grain size, d_{90} than d_{50} (Figs. 5c and 6c). In Fig. 6c, the difference in d_{90} between the prototype and Test 4 at the distal location is pronounced compared to that in d_{50}. It can be inferred that the changes in grain size of the coarse grains e.g., d_{90} at somewhat distal locations serve as a better geomorphic indicator of an increase in overflow velocity.

4.4 Input grain size

Increasing grain size d_{50} = 0.125 mm to 0.25 mm in Test 5 constructs a steeper slope of the levee as a consequence of faster settlement of coarser grains near the channel-floodplain boundary than Test 1 (Fig. 3d). This result can corroborate the previous field observations in Cazanacli and Smith (1998) that coarser levees are likely to be steeper compared to finer levees. Here, note that we increase the near-bed grain size of the channel and Rouse Eq. (2) determines the grain-size distribution and sediment supply rate to the floodplain (Fig. 2). The sediment mixture for Test 5 supplied to the floodplain has a higher peak at the median grain size with a narrow distribution, which drives an abrupt rollover point of d_{90} at the proximal location (Fig. 5d). Since the rollover point of d_{90} means that the coarser grain sizes are more rapidly consumed at the proximal location, the grain size d_{90} declines toward the distal location and the difference in d_{90} between Tests 1 and 5 also becomes similar to that of d_{50} at the distal location (Fig. 6d). Moreover, the sediment concentration in the top of the channel becomes smaller than Test 1 since coarser grains are located in the most bottom part of the Rouse profile, which causes a smaller sediment supply toward the floodplain. The decreasing sediment supply rate in Test 5 consequently leads to lower aggradation rates and thus a longer run time compared to Test 1 (Fig. 4d). However, considering the total sediment volume under the steep

https://doi.org/10.5194/esurf-2021-92
Preprint. Discussion started: 2 December 2021

Earth Surface Dynamics Discussions
Open Access
EGU

levee profile, Test 5 would build the levee until the crest reaches 2 m high with a smaller total sediment amount (i.e., a shorter total run time if the sediment supply rate is equal).

4.5 Control of levee geometry on river avulsion

Based on the findings from the current model, we here estimate a possible linkage between avulsion frequency and levee geometry under given flood and grain-size conditions and explore subsequent associations of levee geometry with river avulsion styles. As the river avulsion is known to be highly sensitive to the depositional patterns and adjacent floodplain morphology (Hajek and Edmonds, 2014; Jerolmack and Mohrig, 2007; Mohrig et al., 2000; Slingerland and Smith, 2004), this section can provide the first-order role of levee morphodynamics in the avulsion processes and, in turn, a source of insight regarding alleviation of damages from natural hazards related to river avulsion.

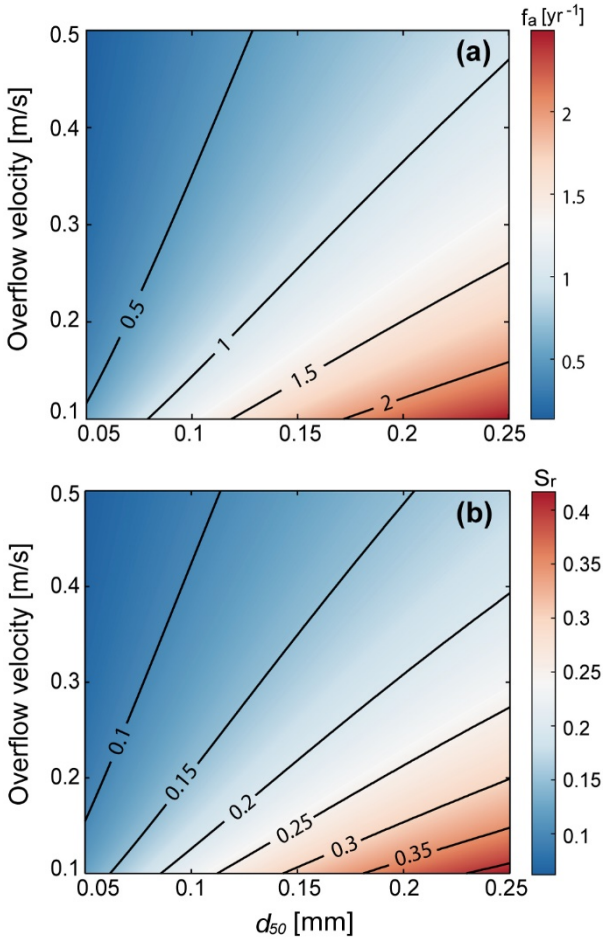

Figure 7. Modelling results for (a) avulsion frequency, f_a and (b) characteristic slope of levee, S_l as a function of the overflow velocity and input median grain size toward the floodplain. We set the intermittency factor, $I_f = 0.02$ for all model runs.

https://doi.org/10.5194/esurf-2021-92
Preprint. Discussion started: 2 December 2021

315 **4.5.1 Avulsion frequency vs. levee slope**

It is generally accepted that natural levee growth acts as an avulsion threshold (Jones and Schumm, 1999) whereby avulsion can initiate when an adjacent levee crest elevates one channel depth in rivers, which is defined as a critical superelevation (Bryant et al., 1995; Jobe et al., 2020; Mohrig et al., 2000). We apply this avulsion threshold to further quantify the avulsion frequency in our numerical modelling by measuring the total run time until the levee crest reaches one channel
320 depth (Fig. 7a). A total 20,050 of levee models are replicated with ranges of the overflow velocities ($U_f = 0.1 \sim 0.5$ m s^{-1}) and median grain sizes supplied into the floodplain ($d_{50} = 0.05 \sim 0.25$ mm), both of which exert important control over the levee geometry as Mohrig et al. (2000) and Jobe et al. (2020) postulated that superelevation is geometrically involved with levee slope (Fig. 7b). A characteristic levee slope is defined here at an avulsion by using the total sediment volume under the levee profile as ${H_c}^2/(2 \times \sum_{i=1}^{N} \eta_i \cdot dx)$, even for the exceptional cases where the levee extends beyond the initial modelling
325 floodplain width of 200 m. Here, we employ the constant water depth case and the total suspended sediment flux into the floodplain of 0.0003 m^2/s. The entrainment effect is ignored for simplicity since neither of them significantly change the final levee geometry. We also assign a flood intermittency factor (I_f) of 0.02, assuming a flood recurrence interval of 3 years documented in Wyżga (1999) and floods lasting about 30 days at a time.

4.5.2 Scaling analysis of avulsion frequency

330 To elucidate the correspondence between the levee geometry and avulsion frequency, we explore here through the use of geometric scaling analysis of avulsion frequency. Avulsion time scale, T_a is estimated in the previous studies (Chadwick et al., 2020; Jerolmack and Mohrig, 2007) as the time required levee crest height to reach the critical superelevation equal to one channel depth, H_c. In this sense, the avulsion frequency (f_a) is given by

$$f_a = I_f \cdot \frac{1}{T_a} = I_f \cdot \frac{v_a}{H_c}, \tag{10}$$

335 where I_f is the intermittency of floods, v_a is the aggradation rate of levee crest during floods which is of the order of $\bar{C}_f w_s$ adopting the characteristic scales $\bar{C}_f$ and w_s for the average sediment concentration in overflow and the settling velocity of median grain size, respectively. If the sediment is transported dominantly in suspension, the sediment flux q_s scales with $\bar{C}_f U_f H_f$ where U_f and H_f are the overflow velocity and depth, respectively. Thus, we roughly rearrange Eq. (10) as

$$f_a \sim I_f \cdot \frac{\bar{C}_f w_s}{H_c} \sim I_f \cdot \frac{q_s w_s}{U_f H_f H_c}. \tag{11}$$

340 As noted in the previous Sect. 4.5.1, approximating the levee shape as a right triangle, the total sediment deposited in the levee that reaches the superelevation can be represented with the characteristic levee slope, S_l:

$$q_s \cdot T_a = \sum_{i=1}^{N} \eta_i \cdot dx = \frac{{H_c}^2}{2 \cdot S_l}. \tag{12}$$

https://doi.org/10.5194/esurf-2021-92
Preprint. Discussion started: 2 December 2021

On the left side of Eq. (12), $T_a = I_f/f_a$ as in Eq. (10) so the avulsion frequency can also be rewritten as

$$f_a = I_f \cdot \frac{2q_s S_l}{{H_c}^2}. \quad (13)$$

The foregoing analyses in Eq. (11) through (13) imply that the avulsion frequency is subjected to the characteristic levee slope (S_l), grain-settling velocity (w_s), and overflow discharge ($U_f H_f$). We can also infer that the characteristic levee slope is proportional to the settling velocity of median grain size and water depth, and is inversely related to the overflow discharge ($S_l \sim \frac{w_s H_c}{U_f H_f}$), which well support the similarity in the trend between the characteristic levee slope and avulsion frequency in Fig. 7. In addition, the settling velocity in Ferguson and Church (2004) derived from Stokes' law follows the relation of $w_s \sim d^2$ and thus the levee slope as well as avulsion frequency is nonlinearly related to the median grain size.

Through the results of our numerical modelling and scaling analysis, it turns out that in the alluvial ridges, not only the critical superelevation is associated with the avulsion threshold, but the characteristic levee slope should be also taken into account in the avulsion processes. Some researchers suggested a floodplain slope ratio as an alternative approach for an avulsion criterion (Guccione et al., 1999; Jones and Schumm, 1999; Mackey and Bridge, 1995; Slingerland and Smith, 1998, 2004; Tornqvist and Bridge, 2002). The floodplain slope ratio is measured as a cross-valley slope relative to the down-channel or down-valley slope. In a large sense, the characteristic levee slope can be a proxy for the cross-valley component of the floodplain slope ratio. These avulsion controls, the floodplain slope ratios and superelevation from the modern rivers, are compared in the study by Mohrig et al. (2000). The authors observed that the normalized superelevation heights are less scatter than the floodplain slope ratios. This scatteredness compared to that in the levee to downstream slope ratios is even up to two orders of magnitude less (Mohrig et al., 2000), but still exists, and can be further explained by our relationship between the avulsion frequency and levee geometry. As in previously published studies (Bryant et al., 1995; Mackey and Bridge, 1995), a high sedimentation rate in the main channel leads to a high avulsion frequency. In this instance, the alluvial ridges would rapidly get toward the local superelevation and build steep slopes in levees as also in our modelling results (see Fig. 7). The channel in turn jumps into a new flow path before preferentially constructing the distal part of the levee (i.e., back loading) and relatively steep levees remain in the abandoned channel producing an increment in the floodplain slope ratio variations (Filgueira-Rivera et al., 2007). Hence, instead of adopting a single criterion, it is reasonable that both the superelevation and characteristic levee slope are taken into account to evaluate the channel avulsion processes (Tornqvist and Bridge, 2002).

4.5.3 Channel reoccupation vs. levee slope

When a river avulsion occurs, flow typically migrates into a preexisting channel or excavates a new flow path in the vicinity of a parent channel searching for low spots with the highest gradient advantage across a basin (Sahoo et al., 2020). In the sense that the former channels can serve as "attractors" to avulsing channels (Heller and Paola, 1996; Jerolmack and Paola, 2007; Mohrig et al., 2000; Reitz et al., 2010; Slingerland and Smith, 2004), it is common to recognize that most avulsion paths are prone to reoccupying the previously abandoned channels in the avulsion history and modern rivers such as the Mississippi

https://doi.org/10.5194/esurf-2021-92
Preprint. Discussion started: 2 December 2021

and Red River avulsion (Aslan et al., 2005; Hajek and Edmonds, 2014; Jerolmack and Paola, 2007). Hajek and Wolinsky (2012) propounded that the extent of proximal levee deposits located along the channel margin may somewhat have an influence on the avulsion behaviour. We therefore conclude that the levee geometry of the active channel may has a strong linkage to the avulsion processes, and the levee geometry of abandoned channels may also have a critical role on the distribution of sediment in the floodplain containing previous channels. It means, depending on the shape of the remnant levees, they can act to barricade the precedently occupied channels (Mohrig et al., 2000).

One of the avulsion types sorted by previous workers is a "local avulsion", where a newly formed channel reverts back to its parent channel or a floodplain channel short distance downstream (Heller and Paola, 1996; Mackey and Bridge, 1995). As maintaining topographic lows and having more erodible materials than nearby floodplain substrates, lately abandoned channels readily capture the flow and coalescence it with any local descent along their bank (Hajek and Wolinsky, 2012; Mohrig et al., 2000). In the case of a relatively steep levee slope, the abandoned channel topography can be protected by the high gradient levees which prevent the influx of flood deposits. Furthermore, the steeper levees are associated with higher avulsion frequency, as described in Eq. (13), which means the avulsion would happen faster and leave the abandoned channel with less time to be filled. If so, it may increase the possibility for an active channel to find the topographic lows of an preexisting channel and reoccupy it as a local avulsion. This style of avulsion especially occurs in tributary systems and produces clustered or superimposed channel sandstone bodies in the stratigraphic records (Hajek and Wolinsky, 2012; Heller and Paola, 1996).

In constrast, if an avulsed channel randomly creates a new pathway across the floodplain rather than reroutes flow back to the previously established channels, it is defined as a "regional avulsion" (Heller and Paola, 1996; Jerolmack and Paola, 2007; Mackey and Bridge, 1995). Once the abandoned channel topography is erased (i.e., smoothed by deposition), it tends to be left out for a long time deprived of any chance to encounter the active channels (Jerolmack and Paola, 2007). Eventually, a new channel is built primarily in the fluvial distributary system or crevasse splays, affecting the downstream channel belt on a large scale, sometimes accompanied by smaller local avulsions (Heller and Paola, 1996). Such avulsion styles are thus susceptible to the floodplain topography and surface roughness, e.g., depressions on the floodplain (Hajek and Edmonds, 2014; Hajek and Wolinsky, 2012; Jerolmack and Paola, 2007; Mohrig et al., 2000; Slingerland and Smith, 2004). With the gentler levees, abandoned channels can be more vulnerable to being modified and smoothed, which is called "channel healing" or "annealing" as opposed to preserve the former topography (Guccione et al., 1999; Reitz et al., 2010; Slingerland and Smith, 2004). The low avulsion frequency predicted by Eq. (13) also intensifies topographic healing on the abandoned channels by providing enough time for the deposition. Due to a removal of topographic memories, a new channel is thereby more likely to advance randomly or to stay in the parent channel position even over the critical superelevation (Jerolmack and Paola, 2007).

https://doi.org/10.5194/esurf-2021-92
Preprint. Discussion started: 2 December 2021

405 **4.5.4 Field applications for avulsion styles**

The linkage between the levee geometry and avulsion styles is applied to the following two field observations: one is a modern avulsive system and the other is from ancient fluvial strata. The former one, from published data by Valenza et al. (2020), investigated how the channel avulsion style evolves from the upstream to downstream reaches in modern rivers. They quantify 63 avulsions across three sedimentary basins of the Andes, Himalayan, and New Guinean basins and suggest that
410 most avulsions close to the mountain fronts generate local (annexational for their term) styles on braided rivers, while the avulsions of relatively further downstream basins mainly make regional (progradational for their term) avulsions on meandering rivers. Valenza et al. (2020) provided several plausible reasons causing the shift in avulsion style, such as downstream changes in slope and downstream fining caused by selective deposition. Given these two changes, we speculate that the levee geometry may affect their transition from the local to regional styles of avulsion. At the upstream part, any
415 amount of coarser sediment overflows into the adjacent floodplain on account of selective deposition along the main stream. Moreover, a flooding type of upstream is traditionally characterized by intense rainfalls in a short period of time. The localized upstream flooding rapidly rises the overflow depth and pours out into the floodplain so that considerable coarser suspended sediment aggrade on the alluvial ridges. As a result, the upstream flash flooding and coarser grains would form non-cohesive steep slopes of levees which can defend former abandoned channels as topographic lows and create a favorable condition for
420 local avulsions. The fine sediment at the downstream basins, on the constrary, is able to transport across the floodplain for a long duration as the downstream flooding has generally a prolonged inundation period with gradually increased flood level on a large scale. The suspended sediment would spread over a great distance, building cohesive levee deposits with a gentler shape and accelerating a topographic healing of any scours or relic channels on the floodplain. By means of the erased topographic memories caused by the gentler-sloped levees, new streams have difficulty reoccupying the abandoned channels.
425 Additionally, cohesiveness of levee deposits due to finer sediment in the downstream basins impedes the destruction of the robust previous levees, which in turn will promote more regional avulsions (Valenza et al., 2020).

The latter one is the Upper Cretaceous alluvial to coastal plain deposits of Blackhawk Formation in Wasatch Plateau, Central Utah, USA. Previous studies on this ancient fluvial strata have identified that the fluvial sandbodies in the upper Blackhawk Formation contain vertically stacked and laterally offset channelized patterns in response to large-scale avulsion
430 processes (Flood and Hampson, 2014, 2015; Hampson et al., 2013; Hampson et al., 2012; Sahoo et al., 2020). Sahoo et al. (2020) highlighted that in terms of channelized sand bodies, their internal architectures, paleochannel mobility, and their distribution and stacking patterns in strata are deeply associated with each other. They interpreted that vertically stacking single-story sand bodies indicate channel reoccupations with low channel mobility, and isolated or lateral offset patterns of multilateral sand bodies represent the regional avulsion style with high mobility of channels. In our model, this can be explained
435 as a result of the geomorphic difference in alluvial ridges. Since the channel mobility, M, is defined as a comparison of the avulsion and lateral migration time scale (Jerolmack and Mohrig, 2007), it is possible that the channel mobility affects the formation of levee shape which is negatively correlated with the avulsion time scale as presented in Eq. (12). We would surmise

https://doi.org/10.5194/esurf-2021-92
Preprint. Discussion started: 2 December 2021

that high channel lateral mobility could allow relatively short time for levees to build only gentler slope, whereas low channel lateral mobility could give enough time to build relatively steeper levees. This brings us a new potential linkage between the channel lateral mobility and avulsion style s(also channel stacking patterns). Yet, it goes quite far beyond the scope of this paper and may bring another great future research topic that requires more confirmation based on field measurements. Furthermore, if we are able to recognize detailed floodplain internal architectures and alluvial ridge configurations in the stratigraphic records, it would be much easier to re-establish the ancient floodplain conditions, e.g., water and sediment supply into the floodplain. Although more field investigations need to be undertaken to verify our hypotheses, the levee stratigraphic records that have been less of interest may still give us practical hints in predicting and reconstructing the river systems related to avulsion processes.

5 Conclusions

The fluvial levee evolution under various boundary conditions was investigated by using the numerical levee-building model with the advection settling of suspended sediment. The current levee-building model allows us to establish what determines the levee geometry and understand the relationship between the levee geometry and avulsion behaviours. Briefly, our main conclusions can be summarized as follow:

1. Overflow discharge and incoming sediment grain size into floodplain exert first-order controls on the levee geometry. The results reflect that relatively gentler shape of levee is associated with faster flooded flow and steeper slope is associated with coarser suspended sediment. The levee geometry can work as a good indicator of paleo-environment in the stratigraphic records.
2. There is a significant correlation between the avulsion frequency and levee geometry in respect of overflow properties. The avulsion frequency is proportional to the characteristic levee slope and median grain size of supplied suspended sediment but nagatively correlated with overflow discharge. With a high avulsion frequency, a steeper levee is more likely to lead reoccupation of the channel to the previoius path indicating a local avulsion. On the other hand, a gentler levee with low frequency causes smooth topography in the abandoned channel, and then a new path would be randomly chosen (i.e., regional avulsion).
3. Our findings are in good agreement with the modern avulsive system reported by Valenza et al. (2020). From upstream to downstream, the levee geometry which can change downstream due to downstream fining and decreasing stream power, is potentially involved in the shift of the avulsion style from local to regional avulsions. We further suggest that the geomorphic difference in alluvial ridges may be related to the channel mobilities and their stacking patterns of sandbodies and explain the case of the upper Cretaceous Blackhawk Formation in Wasatch Plateau, Central Utah, USA described in Sahoo et al. (2020). Even though more field data will be needed to fully test our hypotheses, we can nourish our knowledge of the avulsion processes linking with the levee geometry. Therefore, this

https://doi.org/10.5194/esurf-2021-92
Preprint. Discussion started: 2 December 2021

implies that additional studies of levees are required in order to better predict the avulsion behaviours and their flood risks.

Appendix A: Notation

The following list includes variables with symbols L, M, and T, representing dimensions of length, mass, and time, respectively.

a Reference near bed height, [L].

$\bar{C}_a$ Near bed concentration at $z = a$ in channel, [ ].

$\bar{C}_b$ Near bed concentration in floodplain, [ ].

$\bar{C}_c$ Suspended sediment concentration in channel, [ ].

$\bar{C}_f$ Suspended sediment concentration in floodplain, [ ].

D_s Depositional rate, [L T^{-1}].

d_i ith grain size, [L].

d_{50} Median grain size, [L].

E_i Dimensionless entrainment rate of ith grain size, [ ].

E_s Entrainment rate, [L T^{-1}].

E_{ui} Dimensionless entrainment rate of ith grain size per unit area, [ ].

F_i ith grain size fraction, [ ].

f_a Avulsion frequency, [T^{-1}]

g Gravitational acceleration, [L^2 T^{-1}].

H_c Channel depth, [L].

H_f Overflow depth, [L].

I_f Flood intermittency, [ ].

L Levee length, [L].

P_i Rouse number, [ ].

q_s Volume transport of suspended sediment per unit width, [L^2 T^{-1}].

q_{so} Total sediment flux at the channel-floodplain boundary, [L^2 T^{-1}].

q_{ts} Total sediment flux, [L T^{-1}].

q_w Water flux, [L T^{-1}].

R Submerged specific gravity, [ ].

Re_{pi} Renold's particle number, [ ].

S_f Initial slope of floodplain, [ ].

S_c Initial slope of main channel, [ ].

https://doi.org/10.5194/esurf-2021-92
Preprint. Discussion started: 2 December 2021

S_l	Characteristic slope of levee deposit, [ ].
T_a	Avulsion time scale, [T].
t	Time, [T].
U_f	Overflow velocity, [L T^{-1}].
u_*	Shear velocity, [L T^{-1}].
u_{*s}	Shear velocity associated with skin friction, [L T^{-1}].
v_a	Aggradation rate of levee crest, [L T^{-1}].
w_s	Particle settling velocity, [L T^{-1}].
x	Coordinate to the distal direction of floodplain, [L].
z	Reference elevation, [L].
Z_{ui}	Similarity variable for the ith grain-size range, [ ].
η	Bed elevation, [L].
η_i	Elevation of ith node, [L].
σ	Standard deviation, [ ].
κ	Von Karman constant, [ ].
λ_m	Straining parameter, [ ].
λ_p	Porosity of deposition, [ ].
ν	Kinematic viscosity of fluid, [L^2 T^{-1}].
ρ_s	Sediment density, [M L^{-3}].
ρ_w	Water density, [M L^{-3}].

Code availability

The code used in the one-dimensional levee-building model, associated tests, and its output dataset are openly available at https://github.com/JeongYeonHan/Han2021-LeveeBuildingModel.

Author contribution

JH designed, conducted the computer code with the help of WK; analysed the model results; and wrote the manuscript. WK motivated, conceptualized the study; developed methodology; acquired funding and supervised the research; and revised the paper. Both authors contributed to the discussion and editing of the manuscript writing.

https://doi.org/10.5194/esurf-2021-92
Preprint. Discussion started: 2 December 2021

480 **Competing interests**

The authors declare that they have no conflict of interest.

Acknowledgements

This research was supported by the Basic Science Program through the National Research Foundation of Korea (NRF-2020R1A2C1006083 and NRF-2017R1A6A1A07015374) and in part by the Yonsei University Research Fund of 2021 (2020-
485 22-0507).

References

Adams, P. N., Slingerland, R. L., and Smith, N. D.: Variations in natural levee morphology in anastomosed channel flood plain complexes, Geomorphology, 61, 127-142, doi: 10.1016/j.geomorph.2003.10.005, 2004.

Allen, J. R. L.: A Review of the Origin and Characteristics of Recent Alluvial Sediments, Sedimentology, 5, 89-191, doi:
490 10.1111/j.1365-3091.1965.tb01561.x, 1965.

Aslan, A., Autin, W. J., and Blum, M. D.: Causes of river avulsion: insights from the late Holocene avulsion history of the Mississippi River, USA, Journal of Sedimentary Research, 75, 650-664, doi: 10.2110/jsr.2005.053, 2005.

Brierley, G. J., Ferguson, R. J., and Woolfe, K. J.: What is a fluvial levee?, Sedimentary Geology, 114, 1-9, doi: 10.1016/S0037-0738(97)00114-0, 1997.

495 Bryant, M., Falk, P., and Paola, C.: Experimental study of avulsion frequency and rate of deposition, Geology, 23, 365-368, doi: 10.1130/0091-7613(1995)023<0365:Esoafa>2.3.Co;2, 1995.

Cazanacli, D. and Smith, N. D.: A study of morphology and texture of natural levees - Cumberland Marshes, Saskatchewan, Canada, Geomorphology, 25, 43-55, doi: 10.1016/S0169-555x(98)00032-4, 1998.

Chadwick, A. J., Lamb, M. P., and Ganti, V.: Accelerated river avulsion frequency on lowland deltas due to sea-level rise,
500 Proc Natl Acad Sci U S A, 117, 17584-17590, doi: 10.1073/pnas.1912351117, 2020.

Ferguson, R. I. and Church, M.: A Simple Universal Equation for Grain Settling Velocity, Journal of Sedimentary Research, 74, 933-937, doi: 10.1306/051204740933, 2004.

https://doi.org/10.5194/esurf-2021-92
Preprint. Discussion started: 2 December 2021

Ferguson, R. J. and Brierley, G. J.: Levee morphology and sedimentology along the lower Tuross River, south-eastern Australia, Sedimentology, 46, 627-648, doi: 10.1046/j.1365-3091.1999.00235.x, 1999.

Filgueira-Rivera, M., Smith, N. D., and Slingerland, R. L.: Controls on natural levée development in the Columbia River, British Columbia, Canada, Sedimentology, 54, 905-919, doi: 10.1111/j.1365-3091.2007.00865.x, 2007.

Flood, Y. S. and Hampson, G. J.: Facies And Architectural Analysis To Interpret Avulsion Style and Variability: Upper Cretaceous Blackhawk Formation, Wasatch Plateau, Central Utah, U.S.A, Journal of Sedimentary Research, 84, 743-762, doi: 10.2110/jsr.2014.59, 2014.

Flood, Y. S. and Hampson, G. J.: Quantitative Analysis of the Dimensions and Distribution of Channelized Fluvial Sandbodies Within A Large Outcrop Dataset: Upper Cretaceous Blackhawk Formation, Wasatch Plateau, Central Utah, U.S.A, Journal of Sedimentary Research, 85, 315-336, doi: 10.2110/jsr.2015.25, 2015.

Garcia, M. and Parker, G.: Entrainment of Bed Sediment into Suspension, Journal of Hydraulic Engineering, 117, 414-435, doi: 10.1061/(asce)0733-9429(1991)117:4(414), 1991.

Guccione, M., Burford, M., and Kendall, J.: Pemiscot Bayou, a large distributary of the Mississippi River and a possible failed avulsion, Fluvial sedimentology VI, 28, 211-220, doi: 10.1002/9781444304213.ch16, 1999.

Gugliotta, M., Saito, Y., Ben, B., Sieng, S., and Oliver, T. S. N.: Sedimentology of Late Holocene fluvial levee and point-bar deposits from the Cambodian tract of the Mekong River, Journal of the Geological Society, 175, 176-186, doi: 10.1144/jgs2017-047, 2018.

Hajek, E. A. and Edmonds, D. A.: Is river avulsion style controlled by floodplain morphodynamics?, Geology, 42, 199-202, doi: 10.1130/g35045.1, 2014.

Hajek, E. A. and Wolinsky, M. A.: Simplified process modeling of river avulsion and alluvial architecture: Connecting models and field data, Sedimentary Geology, 257-260, 1-30, doi: 10.1016/j.sedgeo.2011.09.005, 2012.

Hampson, G. J., Jewell, T. O., Irfan, N., Gani, M. R., and Bracken, B.: Modest Change In Fluvial Style With Varying Accommodation In Regressive Alluvial-To-Coastal-Plain Wedge: Upper Cretaceous Blackhawk Formation, Wasatch Plateau, Central Utah, U.S.A, Journal of Sedimentary Research, 83, 145-169, doi: 10.2110/jsr.2013.8, 2013.

Hampson, G. J., Royhan Gani, M., Sahoo, H., Rittersbacher, A., Irfan, N., Ranson, A., Jewell, T. O., Gani, N. D. S., Howell, J. A., Buckley, S. J., and Bracken, B.: Controls on large-scale patterns of fluvial sandbody distribution in alluvial to coastal

plain strata: Upper Cretaceous Blackhawk Formation, Wasatch Plateau, Central Utah, USA, Sedimentology, 59, 2226-2258, doi: 10.1111/j.1365-3091.2012.01342.x, 2012.

Heller, P. L. and Paola, C.: Downstream changes in alluvial architecture: An exploration of controls on channel-stacking patterns, Journal of Sedimentary Research, 66, 297-306, doi: 10.1306/d4268333-2b26-11d7-8648000102c1865d, 1996.

Imran, J., Parker, G., and Katopodes, N.: A numerical model of channel inception on submarine fans, Journal of Geophysical Research: Oceans, 103, 1219-1238, doi: 10.1029/97jc01721, 1998.

James, C. S.: Sediment Transfer to Overbank Sections, Journal of Hydraulic Research, 23, 435-452, doi: 10.1080/00221688509499337, 1985.

Jerolmack, D. J. and Mohrig, D.: Conditions for branching in depositional rivers, Geology, 35, 463-466, doi: 10.1130/g23308a.1, 2007.

Jerolmack, D. J. and Paola, C.: Complexity in a cellular model of river avulsion, Geomorphology, 91, 259-270, doi: 10.1016/j.geomorph.2007.04.022, 2007.

Jobe, Z. R., Howes, N. C., Straub, K. M., Cai, D., Deng, H., Laugier, F. J., Pettinga, L. A., and Shumaker, L. E.: Comparing Aggradation, Superelevation, and Avulsion Frequency of Submarine and Fluvial Channels, Front Earth Sc-Switz, 8, doi: 10.3389/feart.2020.00053, 2020.

Johnston, G. H., David, S. R., and Edmonds, D. A.: Connecting Fluvial Levee Deposition to Flood-Basin Hydrology, J Geophys Res-Earth, 124, 1996-2012, doi: 10.1029/2019jf005014, 2019.

Jones, L. and Schumm, S.: Causes of avulsion: an overview, Fluvial sedimentology VI, 28, 171-178, doi: 10.1002/9781444304213.ch13, 1999.

Mackey, S. D. and Bridge, J. S.: Three-dimensional model of alluvial stratigraphy; theory and applications, Journal of Sedimentary Research, 65, 7-31, doi: 10.1306/d42681d5-2b26-11d7-8648000102c1865d, 1995.

Mishra, K. and Sinha, R.: Flood risk assessment in the Kosi megafan using multi-criteria decision analysis: A hydro-geomorphic approach, Geomorphology, 350, 106861, doi: 10.1016/j.geomorph.2019.106861, 2020.

Mohrig, D., Heller, P. L., Paola, C., and Lyons, W. J.: Interpreting avulsion process from ancient alluvial sequences: Guadalope-Matarranya system (northern Spain) and Wasatch Formation (western Colorado), Geological Society of America Bulletin, 112, 1787-1803, doi: 10.1130/0016-7606(2000)112<1787:Iapfaa>2.0.Co;2, 2000.

555 Pearce, F.: When the levees break, Science, 372, 676-679, doi: doi:10.1126/science.372.6543.676, 2021.

Pierik, H., Stouthamer, E., and Cohen, K.: Natural levee evolution in the Rhine-Meuse delta, the Netherlands, during the first millennium CE, Geomorphology, 295, 215-234, doi: 10.1016/j.geomorph.2017.07.003, 2017.

Pizzuto, J. E.: Sediment Diffusion during Overbank Flows, Sedimentology, 34, 301-317, doi: 10.1111/j.1365-3091.1987.tb00779.x, 1987.

560 Pruszak, Z., Van Ninh, P., Szmytkiewicz, M., Hung, N. M., and Ostrowski, R.: Hydrology and morphology of two river mouth regions (temperate Vistula Delta and subtropical Red River Delta), Oceanologia, 47, doi: 10.1134/S0097807816040084, 2005.

Reitz, M. D., Jerolmack, D. J., and Swenson, J. B.: Flooding and flow path selection on alluvial fans and deltas, Geophysical Research Letters, 37, n/a-n/a, doi: 10.1029/2009gl041985, 2010.

Rouse, H.: Modern conceptions of the mechanics of fluid turbulence, Trans ASCE, 102, 463-505, doi: 10.1061/taceat.0004872,
565 1937.

Sahoo, H., Gani, M. R., Gani, N. D., Hampson, G. J., Howell, J. A., Storms, J. E. A., Martinius, A. W., and Buckley, S. J.: Predictable patterns in stacking and distribution of channelized fluvial sand bodies linked to channel mobility and avulsion processes, Geology, 48, 903-907, doi: 10.1130/g47236.1, 2020.

Skolasińska, K.: Inquiry of levee formation by grain size analysis — A case study from the Warta River (central Poland),
570 Catena, 122, 103-110, doi: 10.1016/j.catena.2014.06.014, 2014.

Slingerland, R. and Smith, N. D.: Necessary conditions for a meandering-river avulsion, Geology, 26, 435-438, doi: 10.1130/0091-7613(1998)026<0435:Ncfamr>2.3.Co;2, 1998.

Slingerland, R. and Smith, N. D.: River Avulsions and Their Deposits, Annual Review of Earth and Planetary Sciences, 32, 257-285, doi: 10.1146/annurev.earth.32.101802.120201, 2004.

575 Smith, N. D. and Pérez-Arlucea, M.: Natural levee deposition during the 2005 flood of the Saskatchewan River, Geomorphology, 101, 583-594, doi: 10.1016/j.geomorph.2008.02.009, 2008.

Tornqvist, T. E. and Bridge, J. S.: Spatial variation of overbank aggradation rate and its influence on avulsion frequency, Sedimentology, 49, 891-905, doi: 10.1046/j.1365-3091.2002.00478.x, 2002.

https://doi.org/10.5194/esurf-2021-92
Preprint. Discussion started: 2 December 2021

Valenza, J. M., Edmonds, D. A., Hwang, T., and Roy, S.: Downstream changes in river avulsion style are related to channel
580 morphology, Nat Commun, 11, 2116, doi: 10.1038/s41467-020-15859-9, 2020.

Wolman, M. G. and Leopold, L. B.: River flood plains: some observations on their formation, doi: 10.3133/pp282C, 1957.

Wyżga, B.: Estimating mean flow velocity in channel and floodplain areas and its use for explaining the pattern of overbank deposition and floodplain retention, Geomorphology, 28, 281-297, doi: 10.1016/S0169-555X(98)00110-X, 1999.